Photolysis of Ketene at 193 nm and the Rate Constant for H + HCCO at 297 K

G. P. Glass,† S. S. Kumaran,‡ and J. V. Michael*

Chemistry Division, Argonne National Laboratory, Argonne, Illinois 60439

Received: February 29, 2000; In Final Form: June 15, 2000

The 193 nm photolysis of ketene was studied by measuring the amount of atomic hydrogen produced when very dilute ketene/Ar and ketene/H_2 mixtures were irradiated by a single pulse from an ArF excimer laser. Absolute concentrations of atomic hydrogen were monitored over a time interval of 0−2.5 ms by using Lyman-α atomic resonance absorption spectroscopy (ARAS). Four different photodissociation channels of ketene were identified: $H_2CCO + h\nu$ gives (a) $CH_2(^3B_1) + CO$; (b) $CH_2(^1A_1) + CO$; (c) HCCO + H; and (d) $C_2O(b^1\Sigma^+) + H_2$. The quantum yields for each channel were measured as $\phi_a = 0.628$, $\phi_b = 0.193$, $\phi_c = 0.107$, and $\phi_d = 0.072$, respectively. To explore the secondary chemistry that occurred when using higher pressure H_2CCO/Ar mixtures, a mechanism was constructed that used well-documented reactions and, for most processes, rate constants that had already been accurately determined. Modeling studies using this mechanism showed the [H] profile to be determined largely by the rate of the reaction H + HCCO → CH_2 + CO. An excellent fit to all of the experimental data was obtained when $k_2 = (1.7 \pm 0.3) \times 10^{-10}$ cm^3 molecule^{-1} s^{-1}.

Introduction

The photolysis of ketene, H_2CCO, has been used as a source of CH_2 for more than 50 years. Most photochemical studies involving H_2CCO have been made using radiation centered in the broad weak absorption band that stretches from 360 to 240 nm, although a few studies have utilized the much stronger diffuse absorption bands that lie between 220 and 190 nm. Two excellent reviews[1,2] summarize much of the early photochemistry.

The lowest energy photodissociation channel for H_2CCO produces triplet methylene with a threshold at 28 250 cm^{-1} above the zero point energy of the ground state of the H_2CCO molecule;[3] i.e.,

$$H_2CCO + h\nu \rightarrow CH_2(^3B_1) + CO$$
$$\Delta E = 28\ 250\ \text{cm}^{-1} \equiv 337.9\ \text{kJ mol}^{-1} \equiv 354\ \text{nm} \quad (1a)$$

The threshold energy for production of the first excited, singlet, state of methylene is 30 116 cm^{-1}.[4]

$$H_2CCO + h\nu \rightarrow CH_2(^1A_1) + CO$$
$$\Delta E = 30\ 116\ \text{cm}^{-1} \equiv 360.2\ \text{kJ mol}^{-1} \equiv 332\ \text{nm} \quad (1b)$$

When H_2CCO is irradiated at wavelengths slightly shorter than that corresponding to this second threshold, both states of CH_2 are produced, but the ratio of singlet to triplet increases rapidly as the energy of the exciting radiation increases.[4] The results of recent measurements of the triplet-to-singlet ratio at 308 nm (the wavelength of a commonly used pulsed laser source) have clustered around a value of 0.06,[5−7] although the value of this ratio was previously a source of some controversy.

At wavelengths shorter than 308 nm (i.e., at higher photolysis energies), other dissociation products become energetically accessible. In 1990, Unfried et al.[8] observed the high-resolution infrared spectrum of the ketenyl radical (HCCO), which was produced in significant amounts when ketene was photolyzed at 193 nm.

$$H_2CCO + h\nu \rightarrow HCCO + H$$
$$\Delta E = 445\ \text{kJ mol}^{-1} \equiv 37\ 200\ \text{cm}^{-1} \equiv 269\ \text{nm} \quad (1c)$$

The HCCO radical plays a significant role in hydrocarbon combustion, where it is produced as a product of the reaction of atomic oxygen with acetylene.[9] In rich flames, HCCO is believed to react with H-atoms, giving $CH_2(^1A_1)$; i.e.,

$$H + HCCO \rightarrow CH_2(^1A_1) + CO \quad (2a)$$

which inserts rapidly into C−H, O−H, and H−H bonds, to produce intermediates that initiate a number of reaction paths leading to higher hydrocarbons and important soot precursors.[9]

The present work was initiated in an attempt to determine the yield of HCCO in the 193 nm photolysis of H_2CCO. No clean source of HCCO is known, and almost all of the known chemistry of this important combustion species has been gleaned by unraveling the complex reaction mechanisms that occur in atomic oxygen−acetylene flames.[10,11] Our initial intention was to determine the ratio of HCCO to $CH_2(^1A_1)$ by measuring the amount of atomic hydrogen produced when a *very* low concentration of H_2CCO was photolyzed in both the presence and absence of a large excess of H_2. In the absence of H_2, atomic hydrogen can be produced *only* by reaction 1c if the H_2CCO concentration is low enough so that secondary reactions cannot occur. In the presence of H_2, additional amounts of atomic hydrogen can be produced by the fast secondary reaction of $CH_2(^1A_1)$ with H_2; i.e.,

* Corresponding author: Phone: (630) 252-3171. Fax: (630) 252-4470. E-mail: Michael@anlchm.chm.anl.gov.

† Visiting Scientist. Permanent address: Department of Chemistry, Rice University, Houston, TX 77251.

‡ Present address: Cabot Corporation, 700 E. US Highway 36, Tuscola, IL 61953.

10.1021/jp000782i CCC: $19.00
Published on Web 08/19/2000

$$CH_2(^1A_1) + H_2 \rightarrow CH_3 + H \quad (3)$$

During the course of the initial experiments, some evidence was obtained that significant amounts of photolysis products other than HCCO and $CH_2(^1A_1)$ were being produced. Therefore, a more comprehensive study, utilizing higher H_2CCO concentrations, was undertaken in order to determine the yield of these products.

Experimental Section

Apparatus. The experiments were performed using a laser photolysis−shock tube (LP−ST) apparatus that has been previously described.[12] In the present instance, all of the data were taken at room temperature, and therefore, the shock tube served simply as a static reaction vessel. The tube was routinely pumped to less than 10^{-8} Torr by an Edwards Vacuum Products Model CR100P packaged pumping system before filling. Radiation (193 nm) was produced by a Questek 2000 excimer laser operating in the ArF mode and was used to photolyze H_2-CCO through a suprasil window in the endplate of the vessel. The H-atom detection technique was atomic resonance absorption spectrometry (ARAS). The laser was operated at 75 mJ. Depending on $[H_2CCO]_0$, this laser pulse gave as much as $[H]_0 \sim 1.5 \times 10^{13}$ atoms cm^{-3} with the photometer positioned 6 cm from the endplate. The absorption path length was 4.2 ± 0.2 cm, and the resonance lamp beam was detected by an EMR G14 solar blind photomultiplier tube. A 4094C Nicolet digital oscilloscope recorded the raw data signals. MgF_2 components were used in the photometer optics.

Gases. Ar and H_2 diluents for the experimental mixtures were obtained from MG Industries, both being Scientific Grade (99.9999%) and used without further purification. Ultrahigh purity grade He (99.999%) for the resonance lamp and high purity H_2 (99.995%) for the atomic filter were from AGA Gases. H_2CCO was prepared from the pyrolysis of diketene[13] and was further purified by bulb-to-bulb distillation in a greaseless, all-glass, high-vacuum gas handling system. The middle third was retained. Mass spectral analysis showed that the sample was >96%, the principal impurity being allene. The photolysis mixtures were accurately prepared from pressure measurements using a Baratron capacitance manometer and were stored in an all-glass vacuum line.

Results

H-Atom Detection. The detection method is H-atom ARAS and has already been fully discussed.[14−17] H-atom Lyman-α emission (121.6 nm) was produced from a 20 W microwave discharge (2450 MHz) in a 2.2 Torr flow of liquid N_2 cooled ultrahigh purity grade He. There are sufficient hydrogen-containing impurities to give a measurable Lyman-α signal. Under these conditions the effective lamp temperature is 420 K, and the line is Gaussian and unreversed;[15,16] i.e., it is only Doppler broadened. The transition at 121.6 nm is spectrally isolated by placing a gas filter section[14] that contains 3 cm of dry air at atmospheric pressure in front of the solar blind photomultiplier. Despite this, some radiation at wavelengths other than 121.6 nm is always present, and it is necessary to determine the fraction of this spectral impurity. Hence, an H-atom filter section is placed in front of the resonance lamp.[18] This filter section consists of a fast discharge-flow system operating with ∼0.2 Torr of H_2. With the flow system microwave discharge operating, sufficient H-atom concentration is produced in the optical path to remove nearly all of the 121.6 nm radiation.[19] The determination of the fraction of light that is resonance radiation is routinely made before each of the present measurements.

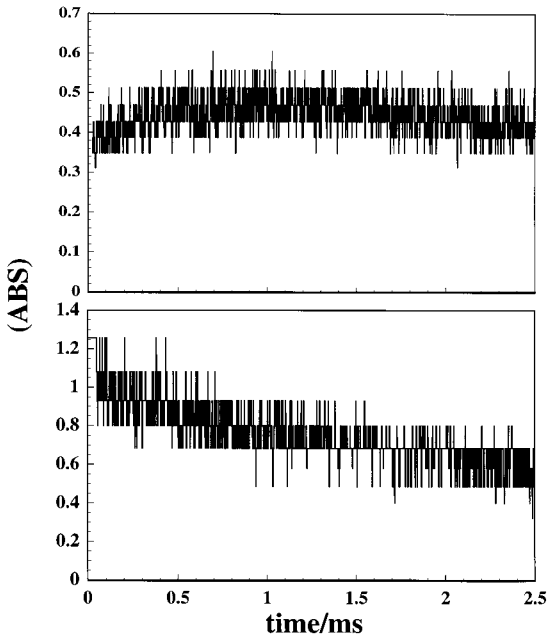

Figure 1. Experimental determination of $(ABS)_t$ at 297 K with FE = 75 mJ for mixtures of H_2CCO in Ar and H_2. Top panel, Ar diluent: $P = 20.17$ Torr and $X_{H_2CCO} = 4.361 \times 10^{-4}$. Bottom panel, H_2 diluent: $P = 20.25$ Torr and $X_{H_2CCO} = 4.272 \times 10^{-4}$.

Low-Pressure Measurements. The yield of H-atoms as a function of $[H_2CCO]_0$ was determined by photolyzing dilute mixtures of H_2CCO ($X \sim 4.3 \times 10^{-4}$) in two bath gases, Ar and H_2, at pressures ranging from 2 to 20 Torr. Figure 1 shows two representative experiments where $(ABS)_t = -\ln(I_t/I_0)$ (I_t and I_0 refer to time-dependent and initial photometric intensities, respectively) is plotted against time. As seen in Figure 1, the overall yield in H_2 is 2−3 times that in Ar. Even at the low H concentration probed with the unreversed source, both mixtures exhibit temporal H concentration behavior on photolysis. The top panel with H_2CCO/Ar shows a slow broad increase of $(ABS)_t$ with increasing time, whereas in the bottom panel with the H_2CCO/H_2 mixture, $(ABS)_t$ decreases slowly with increasing time. These effects are slow enough so that extrapolation to zero time can be easily made, giving fairly accurate values of $(ABS)_0$. Because the oscillator strength for the Lyman-α transition is well-known, absolute H concentrations can be accurately determined from line absorption calculations.[15−17,19] Hence, the curve-of-growth could be determined for a 420 K unreversed source and an absorber at 297 K for a path length of 4.2 cm,[15,16] and the values of $(ABS)_0$ obtained from the present experiments could be converted to absolute $[H]_0$. The resultant $[H]_0$ values are normalized by the flash energy, FE, and are plotted against $[H_2CCO]_0$ in Figure 2.

The top and bottom lines in Figure 2 show the results obtained in the H_2 and Ar mixtures, respectively. With the (0,0) constraint, linear-least-squares analysis gives the equations

$$[H] = (6.64 \pm 0.06) \times 10^{-5} \times FE \times [H_2CCO] \quad \text{in } H_2 \quad \text{(I)}$$

and

$$[H] = (2.06 \pm 0.02) \times 10^{-5} \times FE \times [H_2CCO] \quad \text{in Ar} \quad \text{(II)}$$

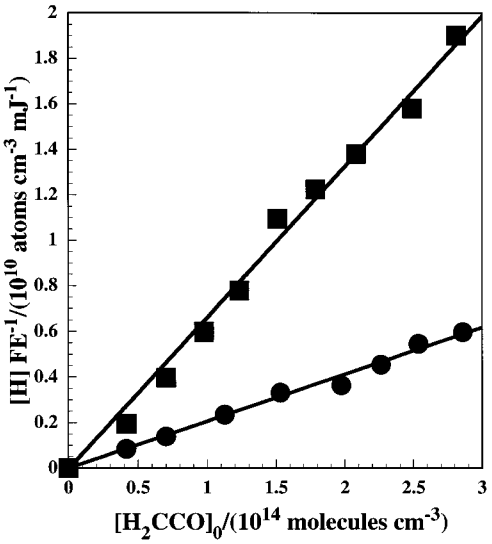

Figure 2. Yields of $[H]_0$ normalized by FE for H_2CCO photolyses in H_2 and Ar diluents at total pressures ranging from ~3−20 Torr: (●) in Ar with $X_{H_2CCO} = 4.361 \times 10^{-4}$; (■) in H_2 with $X_{H_2CCO} = 4.272 \times 10^{-4}$. The linear-least-squares lines are given by eqs I and II.

Hence, the ratio of H-atoms formed when using H_2 as diluent to the H-atoms formed when using Ar as a diluent is 3.19.

Experiments at Higher Pressures. Figure 1 shows kinetics complications in both the Ar and H_2 results. The Ar result shows a formation process with additional atomic hydrogen being formed for ~1 ms from some long-lived intermediate species, whereas the H_2 result shows a continual decay of atomic hydrogen. At the low H_2CCO concentrations used in this and similar experiments, the decay of H observed in mixtures dilute in H_2 cannot be due to H + H_2CCO or to reactions of H with other radicals. Therefore, the observed depletion must be caused by diffusional loss of H-atoms from the viewing zone. The first-order decay constants from the experiments between 3 and 20 Torr have been plotted against inverse pressure, P^{-1}, and from the resulting straight line, a diffusional rate constant of $k_d = 2950\ s^{-1}$ Torr/P has been obtained. The increase of H concentration in the Ar mixture is more complicated and probably involves a kinetically important species reacting with H_2CCO to form H. Clearly, this process requires further consideration, and to systematically investigate it, we decided to carry out kinetics experiments at higher initial values of $[H]_0$ and at pressures greater than ~30 Torr.

Determination of a Curve-of-Growth for a Reversed Source. The unreversed photometer configuration described above is too sensitive for probing higher $[H]_0$, and therefore, as in previous work at room temperature,[15] we had to substantially reduce its sensitivity by using a reversed source, necessitating the determination of a new curve-of-growth. For the new source, we used ultrahigh purity He (99.999%) directly from the cylinder, so that up to 10 ppm of the gas might consist of hydrogeneous impurities. Even though this source is only slightly reversed, the signal-to-noise and decreased sensitivity are sufficient to allow accurate measurements up to $[H]_0 \sim 1.5 \times 10^{13}$ atoms cm^{-3} to be made. The curve-of-growth was determined using $(ABS)_0$ extrapolations in both H_2 and Ar (low P) mixtures at various pressures. In both cases, the corresponding $[H]_0$ values for various $[H_2CCO]_0$ values have been calculated using eqs I or II. The resultant curve-of-growth is shown as Figure 3. The line in the figure is a least-squares polynomial fit to the data (±5% between 5 and 16 × 10^{12} atoms cm^{-3}). Line absorption calculations were then performed using the three layer model previously described[15−17,19] with the H concentration in the source (both plasma and reversal layer) being the only variable parameter. The calculated curve-of-growth (not shown) for [H] = 10 ppm × [He] agreed to within ±13% with the polynomial fit of Figure 3 over the absorber concentration range, (5−16) × 10^{12} atoms cm^{-3}. This indicates remarkably good consistency, since the level of impurities in the source He is reported to be 10 ppm, as noted above.

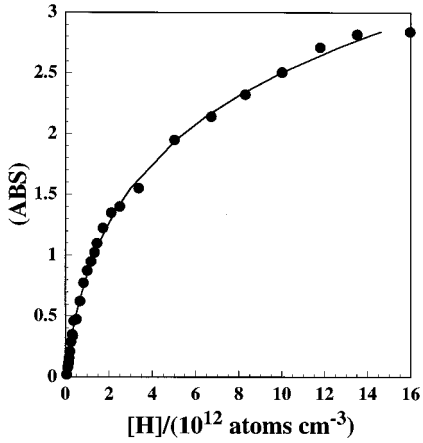

Figure 3. The curve-of-growth for the present reversed source as determined from $(ABS)_0$ extrapolations using measured FE and $[H_2CCO]_0$ in eqs I and II. The line is a least-squares polynomial fit to the data and is within ±5% of the data points at the one standard deviation level.

Kinetics Experiments. Nine kinetics experiments in H_2 and in Ar with $X_{H_2CCO} = 5.173 \times 10^{-4}$ and 5.141×10^{-4}, respectively, have then been performed between 30 and 190 Torr total pressure. Measured values of $(ABS)_t$ have been converted to $[H]_t$ using the curve-of-growth shown in Figure 3. Even though the fit of the curve-of-growth to the data points is within ±5% at the one standard deviation level, it is important to realize that there are other sources of systematic error, the largest being the optical path length in the absorber region, i.e., 4.2 ± 0.2 cm. Data analysis also presumes that there is no variability in the photon flux per unit of laser flash energy. Considering these uncertainties, we consider the error in absolute $[H]_t$ to be ~±15% in the kinetics experiments, even though the relative errors in a given profile may be less. Figure 4 shows typical examples of kinetics profiles in both Ar and H_2.

Discussion

Three different photodissociation channels of H_2CCO, reactions 1b−d,

$$H_2CCO + h\nu \rightarrow C_2O(b^1\Sigma^+) + H_2 \qquad (1d)$$

were identified by the experiments performed at pressures below 20 Torr. Relative quantum yields for each of these channels were determined by measuring the absolute amounts of atomic hydrogen produced in experiments performed at different pressures and with two different diluent gases. Channel 1c was identified by observing $[H]_0$ in low-pressure H_2CCO/Ar mixtures. An unexpected second channel was identified when slightly higher pressure H_2CCO/Ar mixtures were investigated. In these higher pressure mixtures, *additional* H was observed to grow in over a time interval of several hundred microseconds. As the total pressure was systematically increased, this extra concentration of H grew in more rapidly, reaching a maximum at shorter and shorter reaction times. The top panels of Figures 1 and 4 illustrate this behavior.

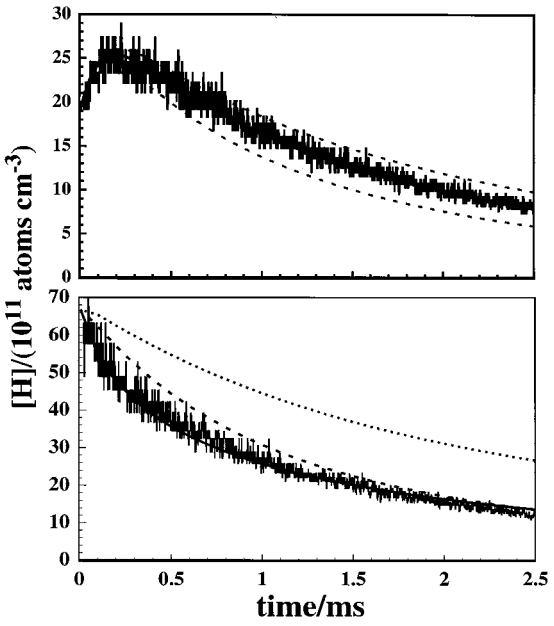

Figure 4. $[H]_t$ profiles in two typical H_2CCO photolysis experiments with FE = 75 mJ and $T = 297$ K. The top panel, in Ar diluent, is with $P = 80.5$ Torr and $X_{H_2CCO} = 5.141 \times 10^{-4}$. The solid line is a simulation using the mechanism of Table 1, and the dashed lines are with $k_2 = k_{2a} + k_{2b}$ halved and doubled. The bottom panel in H_2 diluent is with $P = 80.3$ Torr and $X_{H_2CCO} = 5.173 \times 10^{-4}$. The solid line is a simulation using the mechanism of Table 1. The double-dashed line is a simulation that assumes no photochemical $CH_2(^3B_1)$ production, and the single dashed line is a simulation assuming that there is no photochemical $CH_2(^3B_1)$ production and that $CH_2(^3B_1) + CO$ are the only products from reaction 2.

Using a process of elimination, a possible source of this additional H in the H_2CCO/Ar experiments could be suggested. A secondary reaction of a primary photolysis product had to be responsible for this extra concentration; however, the rate of H-atom formation was much too fast for it to be produced by a reaction of *two* photolysis products, even if these two products were to react on every collision. We therefore concluded that the formation of H had to involve the reaction of a primary photolysis product with the H_2CCO molecule. To identify this primary photolysis product, many possible candidates were considered. Various excited electronic states of H_2CCO were rejected because the ab initio calculations of Allen and Schaefer[20] showed that the lifetimes of all energetically accessible states would be too short to account for our observations. These ab initio calculations identified four excited states that could be reached by using 193 nm photons. The two lowest states ($^3A''$ and $^1A''$) are known to produce $CH_2(^3B_1)$ and $CH_2(^1A_1)$ respectively, and the two higher states ($^3A'$ and $^1B_1$), which we initially considered as possible candidates, appear to have no valid minima. Of the various fragmentation products of electronically excited H_2CCO, $CH_2(b^1B_1)$ was ruled out because its radiative lifetime[21] is less than 10 μs, and vinylidene was dismissed because it is energetically inaccessible. The known reaction of CH with H_2CCO is too fast to account for our observations, and therefore, CH was rejected as a suitable candidate. The only fragmentation candidate remaining is C_2O.

In 1969, based on the photolysis of H_2CCO-D_2CCO mixtures, Laufer[22] suggested that C_2O is produced as a minor (<6%) but primary product in the vacuum ultraviolet photolysis of ketene. The triplet ground state, $C_2O(X^3\Sigma^-)$, is known to react fairly rapidly with H_2, but this species is not sufficiently reactive toward unsaturated hydrocarbons[23] to be the source of the additional H in the present experiments. However, two low-lying singlet states are known to exist, the $C_2O(a^1\Delta)$ state at an energy of 63.3 kJ mol^{-1} and the $C_2O(b^1\Sigma^+)$ state at an energy of 97.7 kJ mol^{-1},[24] both relative to the ground state. Since little is known about the reactivity of either singlet state, and since there are severe energy constraints concerning the production of H from a reaction with ketene, we propose that the higher lying state, $C_2O(b^1\Sigma^+)$, reacts with H_2CCO to form the additional atomic hydrogen in our experiments; i.e.,

$$C_2O(b^1\Sigma^+) + H_2CCO \rightarrow H + CO + HCCCO \qquad (4)$$

Parker et al.[25] investigated the reaction of ground-state $C_2O(X^3\Sigma^-)$ with 2,3-dimethyl-2-butene and proposed an insertion mechanism into the double bond to form a cyclic intermediate. If such an intermediate is formed in reaction 4, it might well fragment as shown above to form the well-characterized[26] radical, HCCCO, and the additional H necessary to explain the H concentration maxima observed in the top panels of Figures 1 and 4. Recent G3 calculations show that reaction 4 with $C_2O(b^1\Sigma^+)$ is exothermic by 24 kJ mol^{-1},[27] although earlier coupled-cluster calculations indicated that it was slightly endothermic.[28] In contrast to reaction 4, reactions of $C_2O(X^3\Sigma^-)$ or $C_2O(a^1\Delta)$ with ketene producing H are both endothermic (i.e., 73.7 and 10.4 kJ mol^{-1}, respectively), provided the products are those shown in reaction 4.

The photolysis of C_3O_2 at 248 nm has been investigated by Becker et al.[29] They concluded that one of the singlet states of C_2O, probably $C_2O(a^1\Delta)$, is formed as an initial photolysis product. This species remained in their system for more than 200 μs, was not noticeably quenched by Ar, but reacted rapidly with C_3O_2. In many ways, its behavior is similar to that observed in our system for the precursor of atomic hydrogen. However, if the products are those shown in reaction 4, we prefer, solely on energetic grounds, to identify the species responsible for H-atom growth in this work to be $C_2O(b^1\Sigma^+)$ rather than $C_2O(a^1\Delta)$. Of course in order for this identification to be correct, one must assume that $C_2O(b^1\Sigma^+)$ is not appreciably quenched to either lower lying state.

The quantum yield of $C_2O(b^1\Sigma^+)$ relative to that of HCCO + H (i.e., ϕ_d/ϕ_c) was determined to be 0.67 by estimating the amount of extra H produced at longer reaction times in experiments similar to those shown in Figures 1 and 4. Modeling studies of the type fully described below were required in order to establish this value.

The yield of channel 1b was measured by comparing the amount of atomic hydrogen formed in dilute, low-pressure H_2CCO/H_2 mixtures with that produced, under similar conditions, in dilute, low-pressure H_2CCO/Ar mixtures. In the presence of several Torr of H_2, 84% of any $CH_2(^1A_1)$ photochemically produced by reaction 1b should react almost instantaneously with H_2 to form H-atoms in reaction 3 with the remaining 16% being collisionally deactivated to $CH_2(^3B_1)$.[30-32] In H_2CCO/H_2 mixtures, the bottom panels of Figures 1 and 4 show that, in the presence of H_2, no additional H is formed, suggesting that $C_2O(^1\Sigma^+)$ reacts with H_2 with a rate constant roughly comparable to that with H_2CCO (i.e., reaction 4). If this were not the case, additional H would be produced as in H_2CCO/Ar. The reaction of $C_2O(^1\Sigma^+)$ with H_2 most likely instantaneously produces yet more H by the direct reaction,

$$C_2O(^1\Sigma^+) + H_2 \rightarrow HCCO + H \qquad (5)$$

although it might be possible that the products of this reaction are $CH_2(^1A_1) + CO$, with H then being produced by reaction 3. Irrespective of which products are formed in reaction 5, the

TABLE 1: Mechanism Used for Fitting H Concentration Profiles after H_2CCO Photolysis at 193 nm

	reaction	k/(cm^3 molecule^{-1} s^{-1})	refs
(2a)	$H + HCCO \rightarrow CH_2(^1A_1) + CO$	$k_{2a} = 1.56 \times 10^{-10}$	10, PW
(2b)	$H + HCCO \rightarrow CH_2(^3B_1) + CO$	$k_{2b} = 1.36 \times 10^{-11}$	11, PW
(3a)	$CH_2(^1A_1) + H_2 \rightarrow H + CH_3$	$k_{3a} = 1.01 \times 10^{-10}$	30, 31[a]
(3b)	$CH_2(^1A_1) + H_2 \rightarrow CH_2(^3B_1) + H_2$	$k_{3b} = 1.92 \times 10^{-11}$	32
(4)	$C_2O(^1\Sigma) + H_2CCO \rightarrow H + CO + HCCCO$	$k_4 = 6.7 \times 10^{-12}$	PW
(5)	$C_2O(^1\Sigma) + H_2 \rightarrow H + HCCO$	$k_5 \geq 1 \times 10^{-12}$	PW
(6)	$CH_2(^3B_1) + H \rightarrow CH + H_2$	$k_6 = 2.25 \times 10^{-10}$	11, 33
(7a)	$CH + H_2 \rightarrow CH_3$	$k_{7a} = 7.2 \times 10^{-30}\rho/(1 + 2.33 \times 10^{-19}\rho)$[b]	34−39
(7b)	$CH + H_2 \rightarrow CH_2(^3B_1) + H$	$k_{7b} = k_6/162$[c]	34−39
(8)	$CH_3 + H \rightarrow CH_4$	$k_8 = -9.37 \times 10^{-12} + 2.92 \times 10^{-29}\rho(1-6.1 \times 10^{-20}\rho)$[b]	40
(9)	$H + H_2CCO \rightarrow CH_3 + CO$	$k_9 = 6.5 \times 10^{-14}$	41
(10a)	$CH + H_2CCO \rightarrow C_2H_2 + H + CO$	$k_{10a} = 2.11 \times 10^{-10}$	42, 43
(10b)	$CH + H_2CCO \rightarrow C_2H_3 + CO$	$k_{10b} = 2.88 \times 10^{-11}$	42, 43
(11)	$CH_2(^1A_1) + Ar \rightarrow CH_2(^3B_1) + Ar$	$k_{11} = 5.5 \times 10^{-12}$	31, 32[a]
(12)	$CH_3 + CH_3 \rightarrow C_2H_6$	$k_{12} = 5 \times 10^{-11}$	44
(13)	$CH_2(^3B_1) + CH_3 \rightarrow C_2H_4 + H$	$k_{13} = 7 \times 10^{-11}$	45
(14)	$CH_2(^3B_1) + CH_2(^3B_1) \rightarrow C_2H_2 + H_2$	$k_{14} = 1.5 \times 10^{-10}$	46−49[a]
(15)	$C_2H_3 + C_2H_3 \rightarrow C_4H_6$	$k_{15} = 1.2 \times 10^{-10}$	50
(16)	$C_2H_3 + H \rightarrow C_2H_2 + H_2$	$k_{16} = 2.0 \times 10^{-10}$	50
(17)	$C_2H_3 + CH_3 \rightarrow C_3H_6$	$k_{17} = 1.2 \times 10^{-10}$	50
(18)	$H \rightarrow {}^1/_2H_2$	$k_{18} = 2950/P$ in H_2 or $1450/P$ in Ar[d]	
(19)	$HCCCO + H \rightarrow C_2H_2 + CO$	$k_{19} = 1.7 \times 10^{-10}$	PW[e]

[a] The value used is an average of the cited references. Other reactions with multiple references are discussed in the text. [b] ρ is total density; k_8 was evaluated from 25 to 206 Torr. [c] 162 is the value of the equilibrium constant at 297 K. [d] k_{18} in s^{-1}. [e] Since no previous value exists for reaction 19, k_{19} is taken to be equal to k_2. PW is present work.

ratio, R, of the $[H]_0$ produced in H_2CCO/H_2 mixtures to that produced in similar H_2CCO/Ar mixtures is given by $R = ((0.84\phi_b) + \phi_c + \phi_d)/\phi_c$, where ϕ_x represents the quantum yield of channel x. R was determined from the ratio of the slopes of the two lines shown in Figure 2 and given in eqs I and II as $(6.64/2.06) = 3.19$. Since $(\phi_d/\phi_c) = 0.67$, it follows that $(\phi_b/\phi_c) = 1.81$.

At higher total pressures, a significant amount of secondary chemistry occurs. To fit measured $[H]_t$ under all conditions, a reaction mechanism was constructed using well-documented reactions. For almost all reactions, rate constants have already been accurately determined in "direct" experiments performed on systems chosen to isolate one individual elementary reaction. In most cases, one or more reactant(s) or product(s) were monitored spectroscopically. This mechanism is shown in Table 1.[33−50]

Following Peeters and co-workers,[10,11] we assumed that H + HCCO, reaction 2, occurs on both singlet and triplet surfaces, producing 92% $CH_2(a^1A_1)$ and 8% $CH_2(X^3B_1)$. The most important reaction that determines $[H]_t$ in H_2CCO/H_2 mixtures is

$$H + CH_2(^3B_1) \rightarrow CH + H_2 \qquad (6)$$

A rate constant was chosen that is 25% greater than that measured by Borland et al.[33] but 20% less than that determined by Boullart and Peeters.[11] CH, from reaction 6, can then react with H_2 and/or H_2CCO; however, the predominant processes with H_2 diluent are the two reactions with H_2 shown in Table 1 as reactions 7a and 7b. The rate constants for these two reactions are based on an evaluated review of previous work[34−36] made by Wagner and Harding.[37] The rate constant for 7a, expressed as a function of density, is a fit to their successful model with $\Delta E_{tot} = -75$ cm^{-1}. Reaction 7b is the reverse of reaction 6, and its rate constant is calculated from 6 using the known equilibrium constant. All three rate constants, from reactions 6, 7a, and 7b, agree well with later work.[38,39] The rate constant for reaction 8 was based on a polynomial fit to the experimental data (25−206 Torr) of Brouard et al.[40] Generally accepted literature values were used for all other available rate constants with one exception, and this is the reaction of CH_3 with $CH_2(^3B_1)$, reaction 13. For this reaction, a rate constant 36% lower than that determined by Deters et al.[45] was chosen.

When fits to the experimental data from H_2CCO/H_2 mixtures were attempted with the model in Table 1, a reasonable fit could not be obtained without assuming some initial photochemical production of $CH_2(^3B_1)$, i.e., without a contribution from channel 1a. The basic problem was that none of the reactions included in the mechanism removed H-atoms at a rate demanded by the experimental data. This situation is illustrated in the bottom panel of Figure 4, where two simulations are shown using different initial assumptions. The double dashed line in the bottom panel shows a fit made under the assumption that $CH_2(^3B_1)$ is not photochemically produced. Clearly, the removal rates are much too slow because reaction 2 (with an assumed value for $k_2 \sim 2 \times 10^{-10}$ cm^3 molecule^{-1} s^{-1}) gives 92% $CH_2(^1A_1)$,[11] which immediately regenerates H in reaction 3a (note that the reaction of $CH_2(^3B_1)$ with H_2 is negligibly slow). The termolecular reaction,[40] $H + CH_3 (+ M) \rightarrow CH_4 (+ M)$, is relatively slow, and the well-known reaction of H with H_2CCO[40] cannot account for more than 15% of the measured H loss. The other simulation in the bottom panel of Figure 4 (single dashed line) shows the prediction under the two assumptions (1) that $CH_2(^3B_1)$ is not photochemically produced and (2) that H + HCCO only gives $CH_2(^3B_1)$ (i.e., reaction 2b is the exclusive pathway), an assumption that rejects the findings of Boullart and Peeters,[11] who obtained experimental results that clearly suggest 92% $CH_2(^1A_1)$ and 8% $CH_2(^3B_1)$ production from reaction 2. This simulation also predicts too shallow a decay curve compared to experiment. Hence, photochemical $CH_2(^3B_1)$ production is necessary in order to fit our experiments using the Table 1 mechanism. As shown below, this conclusion is confirmed by combining the present results with measurements by Hershberger.[51]

The quantum yield of channel 1a was initially chosen to be consistent with the preliminary measurements of Hershberger,[51] who photolyzed H_2CCO at 193 nm in the presence of NO and determined the ratio of $[CH_2]_0/[HCCO]_0$ by measuring infrared absorption due to CO and CO_2. Note that CO_2 is produced in

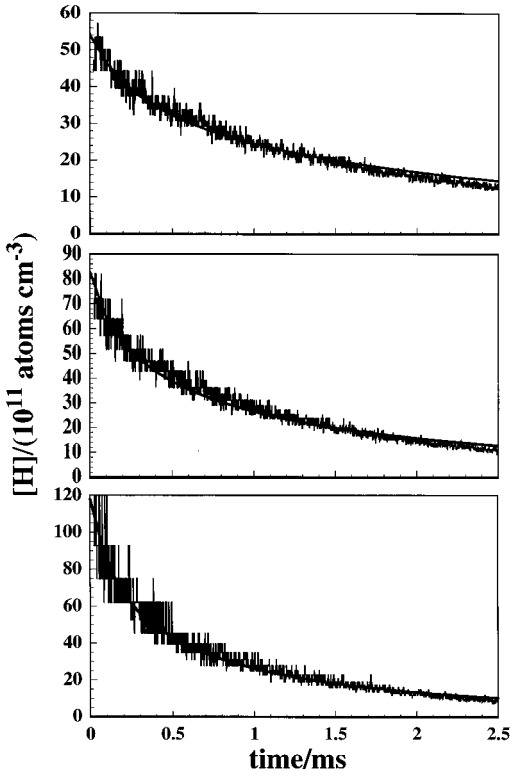

Figure 5. $[H]_t$ profiles in three H_2CCO/H_2 photolysis experiments with $X_{H_2CCO} = 5.141 \times 10^{-4}$, FE = 75 mJ, and $T = 297$ K. The top panel is with $P = 60.0$ Torr, the middle panel is with $P = 99.1$ Torr, and the bottom panel is with $P = 140.8$ Torr. The solid lines are simulations using the mechanism of Table 1.

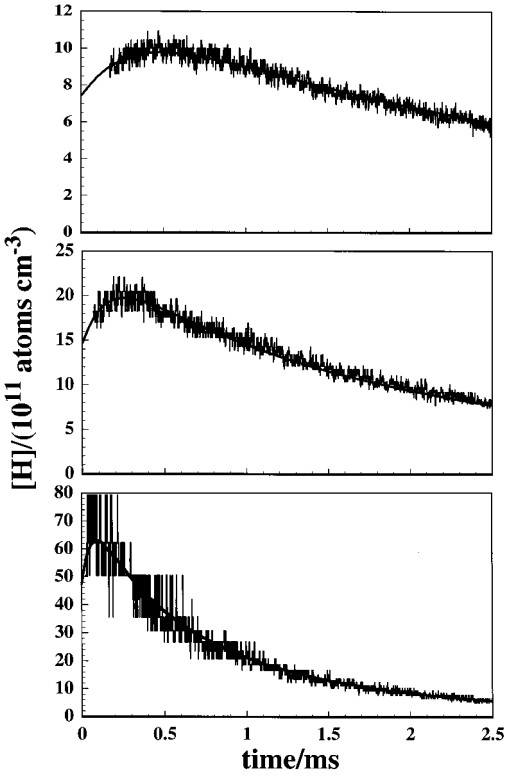

Figure 6. $[H]_t$ profiles in three H_2CCO/Ar photolysis experiments with $X_{H_2CCO} = 5.173 \times 10^{-4}$, FE = 75 mJ, and $T = 297$ K. The top panel is with $P = 29.0$ Torr, the middle panel is with $P = 61.1$ Torr, and the bottom panel is with $P = 162.4$ Torr. The solid lines are simulations using the mechanism of Table 1.

the presence of NO by the reaction

$$HCCO + NO \rightarrow HCN + CO_2 \qquad (20)$$

Hershberger measured $[CH_2]_0/[HCCO]_0 = 5.3$ and equated this value to $(\phi_a + \phi_b)/\phi_c$; however, the possibility of channel 1d was not taken into account. Even though $C_2O(^3\Sigma^-)$ reacts with NO with about the same rate constant[52] as reaction 20,[8] it is unclear if CO and/or CO_2 are products of the reaction. It is our view that the singlet, $C_2O(^1\Sigma^+)$, should not be as reactive toward NO as the triplet, $C_2O(^3\Sigma^-)$. Since $C_2O(^1\Sigma^+)$, as noted above, is the most likely photolysis product, we can agree with Hershberger's neglect of reaction 1d and subsequent conclusion. If the above derived ratios for the other primary processes are combined with $(\phi_a + \phi_b)/\phi_c = 5.3$ and $(\phi_a + \phi_b + \phi_c + \phi_c) = 1$, then $\phi_a = 0.501$, $\phi_b = 0.260$, $\phi_c = 0.143$, and $\phi_d = 0.096$ are obtained. These values were initially used to model the experiments using the Table 1 mechanism, but the experiments indicated faster H-atom decay than predicted by the model. Hence, $(\phi_a + \phi_b)/\phi_c$ was eventually modified to 7.7, which then implies $\phi_a = 0.628$, $\phi_b = 0.193$, $\phi_c = 0.107$, and $\phi_d = 0.072$. These quantum yield values were then used to fit all of the data in both H_2 and Ar diluents.

For all simulations, the initial concentrations of CO, $CH_2(^1A_1)$, $CH_2(^3B_1)$, C_2O, and HCCO are determined from $[H]_0$ using the values for the quantum yields for 1a−1d. The initially used $[H]_0$ values are calculated using eqs I or II, and the experiments are simulated using the Table 1 mechanism. Because there are shot-to-shot variations in the laser intensity, the $[H]_0$ values are slightly adjusted in order to obtain the best fits, with the final values generally being within ±10% of the equation inferences. The simulations shown as solid lines in Figure 4 are determined in this fashion. Also Figures 5 and 6 each show three additional simulations in H_2 and Ar diluents, respectively, that span the range of conditions used in the study. The k_2 value that was necessary for fitting these profiles is 1.7×10^{-10} cm^3 molecule^{-1} s^{-1}, partitioned into k_{2a} and k_{2b}, as measured by Peeters and co-workers.[10,11] Hence, this successful value for k_2 represents a relatively direct determination, as will be shown below in connection with the experiments in Ar diluent. The comparisons of predictions to experiments are excellent, with the simulations agreeing with experiments within the experimental accuracy of the $[H]_t$ analysis, i.e., ±15%. Since experiments performed in different bath gases and at different pressures probe entirely different parts of the overall mechanism, the fact that all of the experimental data can be modeled so accurately by the mechanism listed in Table 1 suggests that much of the chemistry contained in this mechanism is correct.

When using H_2 as a diluent, 80% of the loss of H-atoms that occurs at reaction times shorter than 250 μs is due to reaction 6. Because $CH_2(^3B_1)$ is rapidly lost by reactions 13 and 14, this fraction drops to 30−50% at reaction times of ∼2 ms. It is this second-order loss of $CH_2(^3B_1)$ along with some H formation in reaction 13 that accounts for the characteristic bow shape of the experimental $[H]_t$ values shown in Figures 4 and 5. This behavior is explicitly illustrated with reduced mechanism simulations of the experiment shown in the bottom panel of Figure 4. If a 12-step reduced mechanism that includes only reactions 2a, 2b, 3a, 5, 6, 7a, 8, 9, 12, 13, 14, and 18 is used, then the simulation is within ±2% of the Figure 4 result. This shows that almost all atom−radical and radical−radical reactions are negligible, except reactions 6, 8, and 12−14. If we were to adjust k_{13} so that it lay within the lower limit suggested by Deters et al.,[45] the mechanism could be made to reproduce the experimental results by increasing the value of k_6 by 12%. Such a change would have no discernible effect on the simulations

made to reproduce the experimental data using Ar as a diluent. Additionally, if k_{2a} and $k_{2b} = 0$, then the 10-step mechanism predicts $[H]_t$ to be high by at most 8%. This reiterates the importance of reaction 6 as the major loss process for H and also shows that $[H]_t$ is not sensitive to the title reaction 2 under excess H_2 conditions. Therefore, k_2 cannot be determined in the H_2 diluent experiments.

When using Ar as diluent, a significant fraction (>60%) of H-atom loss occurs as a result of the reactions of H with HCCO, reactions 2a and 2b, and therefore, fits to these experiments allowed for k_2 determinations. $[H]_t$ is also influenced by reaction 6, but the other reactions (particularly, most atom−radical and radical−radical reactions) in Table 1 really have a negligible effect on simulated profiles. A simulation of the top panel experiment in Figure 4 using the reduced mechanism, reactions 2a, 2b, 4, 6, 9, 10a, 10b, 11, and 18, gives a result that is within <0.5% of that with the complete mechanism. Reaction 9 is not major and contributes <15% to the profile. Reaction 18 is likewise unimportant at all pressures. Even though $CH_2(^1A_1)$ is clearly photochemically formed in 1b as indicated from the H_2 data, in the Ar data set, $CH_2(^1A_1)$ is instantaneously converted to $CH_2(^3B_1)$ through reaction 11. Therefore, if only the Ar data had been available, the same profile would have been predicted had we assumed (a) that the only channel for reaction 2 is 2b with a rate constant of 1.7×10^{-10} cm^3 molecule^{-1} s^{-1} and (b) that no $CH_2(^1A_1)$ is ever photochemically formed and that the total quantum yield for $CH_2(^3B_1)$ production is $0.628 + 0.193 = 0.821$. In this event, reaction 11 is unnecessary, and this would then leave only reactions 2b, 4, 6, 10a, and 10b, as the important reactions determining $[H]_t$. Rate constants for 6, 10a, and 10b are well-known.[11,33,42,43] Therefore, the Ar simulations are mostly determined by rate constants for reactions 2b and 4, with 4 dominating in the initial and 2b dominating in the later stages, respectively, of the profile. All of the profiles in Ar diluent require that reaction 4 gives H-atoms, suggesting H + CO + HCCCO products. Fitting then requires values for the quantum yields, particularly for 1d, and mutual variations in two rate constants with three quantities to be optimized (i.e., (1) the initial rate of H-atom formation, (2) the maximum [H], and (3) the time for the maximum to be reached) in 10 experiments. The values for ϕ_d, k_4, and k_2 were thereby obtained, with $\phi_d = 0.072$, $k_4 = 6.7 \times 10^{-12}$, and $k_2 = 1.7 \times 10^{-10}$ (k in units of cm^3 molecule^{-1} s^{-1}) being optimal for the 10 experiments. Regarding reaction 2, Figure 4 shows simulations with k_2 halved and doubled (±50%) from the successful value given in Table 1. We find that simulations with $k_2 \pm 18\%$ are not as good as shown in Figure 4 but are within the upper and lower bounds of the $[H]_t$ signal noise, indicating that $k_2 = (1.7 \pm 0.3) \times 10^{-10}$ cm^3 molecule^{-1} s^{-1}.

The present rate constant for the title reaction can be compared to previously published values. On the basis of earlier work from Van de Ven and Peeters,[53] Boullart and Peeters[11] report $k_2 = 1.73 \times 10^{-10}$ cm^3 molecule^{-1} s^{-1} at room temperature, in good agreement with the present work. On the other hand, Frank et al.[54] have reported a value of 2.5×10^{-10} cm^3 molecule^{-1} s^{-1} for shock tube experiments between 1500 and 2500 K. We note that the title reaction on either the singlet or triplet potential energy surface probably proceeds without activation energy through vibrationally hot ketene. Both dissociation channels are lower lying than the entrance channel in which case forward dissociation to both singlet and triplet methylenes and CO is faster than back dissociation. The lifetime of the vibrationally hot molecule is undoubtedly shorter than collision times, and therefore, this reaction is in the high-pressure limit. High-pressure bimolecular limiting rate constants can be calculated using a Lennard-Jones model.[55] Collision rates between H and HCCO are calculated from the standard expression.[56] The potential parameters for both H and HCCO are derived from polarizabilities by methods described by Hirschfelder et al.[56] These are combined as suggested by Cambi et al.[57] to obtain $\sigma_{H,HCCO} = 3.471$ Å and $\epsilon_{H,HCCO} = 63.762$ K. Calculated collision rates range from 11.2 to 17.9×10^{-10} cm^3 molecule^{-1} s^{-1} between 300 and 2000 K, respectively. Comparison to the experimental value at room temperature would suggest a steric factor of ~0.15. If this factor is constant as a function of temperature, then the predicted value at 2000 K would be $\sim 2.7 \times 10^{-10}$ cm^3 molecule^{-1} s^{-1}. Therefore, the larger value, noted by Frank et al., is consistent with the slight T-dependence predicted from this collision model.

Acknowledgment. The authors would like to thank Dr. B. Ruscic for G3 calculations in connection with reaction 4 and for valuable discussions. We also thank Dr. A. F. Wagner for useful suggestions. This work was supported by the U. S. Department of Energy, Office of Basic Energy Sciences, Division of Chemical Sciences, under Contract No. W-31-109-Eng-38.

References and Notes

(1) Frey, H. M. *Prog. Reaction Kinetics* **1964**, *2*, 131.
(2) DeMore, W. B.; Benson, S. W. *Adv. Photochem.* **1964**, *2*, 219.
(3) Lovejoy, E. R.; Kim, S. K.; Moore, C. B. *Science* **1992**, *256*, 1489.
(4) Kim, S. K.; Choi, Y. S.; Pibel, C. D.; Zheng, Q.-K.; Moore, C. B. *J. Chem. Phys.* **1991**, *94*, 1954.
(5) Hayden, C. C.; Neumark, D. M.; Shobatake, K.; Sparks, R. K.; Lee, Y. T. *J. Chem. Phys.* **1982**, *76*, 3607.
(6) Morgan, C. G.; Drabbels, M.; Wodtke, A. M. *J. Chem. Phys.* **1996**, *104*, 7460.
(7) Wade, E. A.; Clauberg, H., Kim, S. K.; Mellinger, A.; Moore, C. B. *J. Phys. Chem.* **1997**, *101*, 732.
(8) Unfried, K. G.; Glass, G. P.; Curl, R. F. *Chem. Phys. Lett.* **1991**, *177*, 33.
(9) Miller, J. A.; Kee, R. J.; Westbrook, C. K. *Annu. Rev. Phys. Chem.* **1990**, *41*, 345. For a review, see: Michael, J. V.; Wagner, A. F. *J. Phys. Chem.* **1990**, *94*, 2454.
(10) Vinckier, C.; Schaekers, M.; Peeters, J. *J. Phys. Chem.* **1985**, *89*, 508.
(11) Boullart, W.; Peeters, J. *J. Phys. Chem.* **1992**, *96*, 9810.
(12) Michael, J. V. *J. Chem. Phys.* **1989**, *90*, 189.
(13) Andreades, S.; Carlson, H. D. *Org. Synth.* **1973**, *Coll. V*, 679.
(14) Barker, J. R.; Michael, J. V. *J. Opt. Soc. Am.* **1968**, *58*, 1615.
(15) Lynch, K. P.; Schwab, T. C.; Michael, J. V. *Int. J. Chem. Kinet.* **1976**, *8*, 651.
(16) Maki, R. G.; Michael, J. V.; Sutherland, J. W. *J. Phys. Chem.* **1985**, *89*, 4815.
(17) Lim, K. P. and Michael, J. V. *Proc. Combust. Inst.* **1994**, *25*, 713.
(18) Miller, J. C.; Gordon, R. J. *J. Chem. Phys.* **1983**, *78*, 3713.
(19) Michael, J. V.; Lifshitz, A. *Handbook of Shock Waves*; Academic: New York, 2000, in press.
(20) Allen, W. D.; Schaefer, F. *J. Chem. Phys.* **1986**, *84*, 2212.
(21) Garcia-Moreno, I.; Lovejoy, E. R.; Moore, C. B. *J. Chem. Phys.* **1993**, *98*, 873.
(22) Laufer, A. H. *J. Phys. Chem.* **1969**, *75*, 959.
(23) Williamson, D. G.; Bayes, K. D. *J. Am. Chem. Soc.* **1968**, *90*, 1957. Donnelly, V. M.; Pitts, W. M.; Baronavski, A. P. In *Laser Probes in Combustion Chemistry*; ACS Symp. Ser. 134; Crosley, D. R., Ed.; American Chemical Society: Washington DC, 1980; p 389.
(24) Zengin, V.; Perrson, B. J.; Strong, K. M.; Continetti, R. E. *J. Chem. Phys.* **1996** *105*, 9740.
(25) Parker, G.; Wiseman, D.; Wintner, C.; Mackay, C. *J. Org. Chem.* **1984**, *49*, 4494.
(26) Jiang, Q.; Graham, W. R. M. *J. Phys. Chem.* **1993,** *98*, 9251.
(27) Ruscic, B., private communication, 1999.
(28) Tomasic, Z. A.; Scuseria, G. E. *J. Phys. Chem.* **1991**, *95*, 6905.
(29) Becker, K. H.; König, R.; Mueser, R.; Wiesen, P.; Bayes, K. D. *J. Photochem. Photobiol. A.; Chem.* **1992**, *64*, 1.
(30) Hayes, F.; Gutsche, G. J.; Lawrence, W. D.; Staker, W. D.; King, K. D. *Combust. Flame* **1995**, 100, 653.
(31) Hancock, G.; Heal, M. R. *J. Phys. Chem.* **1992**, 96, 10316.
(32) Bley, U.; Temps, F. *J. Chem. Phys.* **1993**, *98*, 1058.

(33) Borland, T.; Temps, F.; Wagner, H. Gg. *J. Phys. Chem*. **1987**, 91, 1205.
(34) Berman, M. R.; Lin M. C. *J. Chem. Phys.* **1984**, *81*, 5743.
(35) Zabarnick, S.; Fleming, J. W.; Lin. M. C. *J. Chem. Phys.* **1985**, *85*, 4373.
(36) Becker, K. H.; Kurtenbach, R.; Wiesen, P. *J. Phys. Chem*. **1991**, *95*, 2390.
(37) Wagner, A. F.; Harding, L. B. *Isotope Effects in Gas Phase* Chemistry; ACS Symp. Series 502; Kaye, J. A., Ed.; American Chemical Society: Washington DC, 1992; p 48, and a private communication, 1999.
(38) MacIlroy, A.; Tully, F. P. *J. Chem. Phys.* **1993**, *99*, 3597.
(39) Fulle, D.; Hippler, H. *J. Chem. Phys.* **1997**, *106*, 8691.
(40) Brouard, M.; Macpherson, M. T.; Pilling, M. *J. Phys. Chem*. **1989**, *93*, 4047.
(41) Michael, J. V.; Nava, D. F.; Payne, W. A.; Stief, L. J. *J. Chem. Phys*. **1979**, *70*, 5222.
(42) Hancock, G.; Heal, M. R. *J. Chem. Soc., Faraday Trans.* **1992**, *88*, 2121.
(43) Walsh, R.; Frey, H. M. *J. Phys. Chem*. **1985**, *89*, 2445.
(44) Slagle, I. R.; Gutman, D.; Davies, J. W.; Pilling, M. J. *J. Phys Chem*. **1988**, *92*, 2455.
(45) Deters, R.; Otting, M.; Wagner, H. Gg.; Temps, F. *Ber. Bunsen-Ges. Phys. Chem*. **1998**, *102*, 978.
(46) Bauerle, S.; Klatt, M.; Wagner, H. Gg. *Ber. Bunsen-Ges. Phys. Chem*. **1995**, *99*, 870.
(47) Darwin, D. C.; Young, A. T.; Johnson, H. S.; Moore, C. B. *J. Phys. Chem*. **1989**, *93*, 1074.
(48) Darwin, D. C. PhD Thesis, UC Berkeley, 1989.
(49) Carstensen, H.-H. Ph.D. Thesis, University of Gottingen, 1994.
(50) Fahr, A.; Laufer, A.; Klein, R.; Braun, W. *J. Phys. Chem*. **1991**, *95*, 3218.
(51) Hershberger, J. F. *20th Annual Combustion Research Conference*; US Department of Energy, Basic Energy Sciences, June 9, 1999; p 137.
(52) Donnelly, V. M.; Pitts, W. M.; McDonald, J. R. *Chem. Phys.* **1980**, *49*, 289.
(53) Van de Ven, P.; Peeters, J. *Bull. Soc. Chim. Belg.* **1990**, *99*, 509.
(54) Frank, P.; Bhaskaran, K. A.; Just, Th. *Proc. Combust. Inst.* **1988**, *21*, 885.
(55) Kumaran, S. S.; Su, M.-C.; Lim, K. P.; Michael, J. V.; Wagner, A. F.; Harding, L. B.; Dixon, D. A. *J. Phys. Chem.* **1996**, *100*, 7541, and references therein.
(56) Hirschfelder, J. O.; Curtiss, C. F.; Bird, R. B. *Molecular Theory of Gases and Liquids*, Wiley: New York, 1966.
(57) Cambi, R.; Cappelletti, D.; Liuti, G.; Pirani, F. *J. Chem. Phys.* **1991**, *95*, 1852.